INTERFRACTION LIVER SHAPE VARIABILITY AND IMPACT ON GTV POSITION DURING LIVER STEREOTACTIC RADIOTHERAPY USING ABDOMINAL COMPRESSION

Cynthia L. Eccles, B.Sc., **Laura A. Dawson, M.D.**, **Joanne L. Moseley, PH.D.**, and **Kristy K. Brock, PH.D.**
Radiation Medicine Program, Princess Margaret Hospital, and University of Toronto, Toronto, Ontario, Canada

Abstract

Purpose—For patients receiving liver stereotactic body radiotherapy (SBRT), abdominal compression can reduce organ motion, and daily image guidance can reduce setup error. The reproducibility of liver shape under compression may impact treatment delivery accuracy. The purpose of this study was to measure the interfractional variability in liver shape under compression, after best-fit rigid liver-to-liver registration from kilovoltage (kV) cone beam computed tomography (CBCT) scans to planning computed tomography (CT) scans and its impact on gross tumor volume (GTV) position.

Methods and Materials—Evaluable patients were treated in a Research Ethics Board–approved SBRT six-fraction study with abdominal compression. Kilovoltage CBCT scans were acquired before treatment and reconstructed as respiratory sorted CBCT scans offline. Manual rigid liver-to-liver registrations were performed from exhale-phase CBCT scans to exhale planning CT scans. Each CBCT liver was contoured, exported, and compared with the planning CT scan for spatial differences, by use of in house–developed finite-element model–based deformable registration (MORFEUS).

Results—We evaluated 83 CBCT scans from 16 patients with 30 GTVs. The mean volume of liver that deformed by greater than 3 mm was 21.7%. Excluding 1 outlier, the maximum volume that deformed by greater than 3 mm was 36.3% in a single patient. Over all patients, the absolute maximum deformations in the left–right (LR), anterior–posterior (AP), and superior–inferior directions were 10.5 mm (SD, 2.2), 12.9 mm (SD, 3.6), and 5.6 mm (SD, 2.7), respectively. The absolute mean predicted impact of liver volume displacements on GTV by use of center of mass displacements was 0.09 mm (SD, 0.13), 0.13 mm (SD, 0.18), and 0.08 mm (SD, 0.07) in the left–right, anterior–posterior, and superior–inferior directions, respectively.

Conclusions—Interfraction liver deformations in patients undergoing SBRT under abdominal compression after rigid liver-to-liver registrations on respiratory sorted CBCT scans were small in most patients (<5 mm).

Keywords

Liver radiotherapy; Abdominal compression; Deformable registration

INTRODUCTION

The use of stereotactic body radiotherapy (SBRT) to treat unresectable primary and metastatic liver cancers has shown high rates of local control (1–6). Safe delivery of SBRT is ensured by use of image-guided treatment (IGRT) strategies, reproducible patient immobilization, accurate treatment delivery and planning correlations, pretreatment quality assurance, and methods accounting for tumor/organ motion during treatment. A major challenge in achieving safe, accurate liver radiotherapy is defining and limiting respiratory liver motion during treatment. Liver motion occurs primarily in the superior–inferior (SI) direction in the range of 5 to 50 mm (7,8). If not minimized or properly accounted for, motion of this magnitude could lead to adverse radiotherapy planning and delivery effects including the introduction of artifacts on planning computed tomography (CT) scans, inaccurate tumor volumes (9–11), altered dosimetry from use of a static plan (9), an increased volume of normal tissue irradiated (4), the requirement of increased planning target volume margins (12), and greater risk of toxicity.

Methods used to manage and account for respiratory motion include abdominal compression (AC), active breathing coordination (ABC), and respiratory gating (9,13–18). Abdominal compression is a widely reported method used in lung and liver SBRT, and it primarily uses a constant force applied to the abdomen to reduce diaphragmatic motion, which is verified by fluoroscopy (16,19,20). Heinzerling *et al.* (21) and Wunderink *et al.* (22) have reported the reproducibility of respiratory liver and tumor excursion under AC using four-dimensional computed tomography (4DCT) and fluoroscopy. Heinzerling *et al.* evaluated the effect of varying levels of compression on liver motion using 4DCT and determined that high levels of compression improved motion control over medium levels of compression. With gold fiducial markers implanted in healthy liver tissue surrounding the tumor, Wunderink *et al.* determined that AC effectively reduced liver tumor motion, yielding small, reproducible excursions in three dimensions. von Siebenthal *et al.* (23,24) showed that local liver deformations in free-breathing (FB) patients varied depending on location within the liver. The effect of local deformations may be exaggerated or minimized when using AC and the diaphragm as a surrogate for liver motion. To date, no one has reported on the interfraction variability of liver shape and its impact on tumor position during liver SBRT under AC.

The purpose of this study was to measure the residual interfraction variability in liver shape in patients treated with liver SBRT under AC after the elimination of residual positional errors by use of deformable registration for kilovoltage (kV) cone beam computed tomography (CBCT) scans registered to planning CT scans and its impact on gross tumor volume (GTV) position.

METHODS AND MATERIALS

The first 16 patients (Table 1) treated consecutively with AC on local ethics–approved liver SBRT protocols, from July 2004 to May 2007, were evaluated.

All patients evaluated were ineligible for assisted breath hold but showed reduced respiratory liver motion under AC when compared with FB during screening at the time of treatment planning.

Motion assessment

At the time of treatment planning, FB respiratory liver motion was measured by use of anterior–posterior (AP) fluoroscopy as well as cine–magnetic resonance imaging (MRI) and

4DCT whenever feasible. For all patients with more than 5 mm of SI motion, motion management strategies were investigated including ABC and AC.

All patients included in this analysis had greater than 5 mm of FB respiratory motion and were deemed unsuitable for breath-hold radiotherapy because of an inability to repeatedly hold their breath for 15 seconds or more, communication concerns, or unstable breath holds. Patient ABC screening and motion management determination are described elsewhere (17,25,26). For all patients evaluated, AC reduced liver motion when compared with uninhibited FB.

Abdominal compression

Abdominal compression was applied to each patient, by use of one of three systems. Before the acquisition of a commercially available stereotactic body frame (Elekta, Crawley, UK), a foam cushion and patient safety strap were used to apply AC ($n = 2$). Subsequently, a commercial system was used in a limited number of patients ($n = 2$), until a lightweight, easily maneuverable in-house, indexable system was developed and used for the remainder of patients ($n = 12$). Abdominal compression was applied until maximum tolerability was reached as indicated by the patient. Abdominal compression was not used in patients with colostomy or known risk of thrombosis. Asymmetric planning target volume margins using exhale imaging for the baseline liver position were applied for all patients based on the motion seen at treatment planning.

CT simulation

For target delineation, CT simulation was performed with intravenous (IV) contrast (Visipaque 270, Amersham Health, Princeton, NJ) delivered at 3 to 5 mL/s, for a volume of 2 mL/kg up to a maximum of 150 mL, under AC in voluntary exhale breath holds followed by 4DCT for motion evaluation. Images were acquired from 2 to 3 cm superior to the exhale liver to the bony pelvis, and were reconstructed at 2.5 mm.

Cone beam CT imaging

Daily IGRT using orthogonal kV imaging with or without kVCBCT was performed on a CBCT scan–enabled linear accelerator. Fluoroscopic projections were acquired immediately prior to treatment to confirm respiratory motion magnitude under AC, followed by a combination of orthogonal images and volumetric CBCT using extra sampling for offline 4DCT generation. Offline evaluation was performed on CBCT scans reconstructed to generate 10 phase respiratory sorted CBCT scans by use of MATLAB (The MathWorks, Natick, MA), as described by Sonke *et al.* (27).

Registration and segmentations

For each available CBCT scan, the exhale-sorted CBCT scan was exported to the treatment planning system (Pinnacle, version 7.6; Philips Medical Systems, Andover, MA), where manual rigid liver-to-liver registrations to planning CT scans (exhale) were performed, eliminating rigid residual liver position offsets. This method of best-fit liver-to-liver registration was previously described by Hawkins *et al.* (28) and Brock *et al.* (29). After registration, using the Pinnacle segmentation tools, CBCT livers were contoured by a single observer (C.L.E.), initially copying the liver contour from the planning CT scan and then manually morphing it regionally to fit the liver to each CBCT scan to reduce recontouring errors. A 100% match with the planning CT liver was assumed wherever the liver was not well visualized on CBCT. Intraobserver contouring variability was determined by generating three repeat contours on a single CBCT liver scan for three patients. Once the liver contours were complete, they were exported from the treatment planning system to MORFEUS.

Deformable registration—MORFEUS

Evaluation of spatial differences between CBCT and planning CT was done by use of in house–developed finite element model–based deformable registration (MORFEUS) (29–32). MORFEUS is a biomechanical model–based deformable registration tool that uses guided surface projection of organ contours combined with biomechanical properties of tissues as opposed to intensity values to drive registration. This is beneficial for the application of CT to CBCT registration of the liver, given the lack of soft-tissue contrast, including visibility of the tumor, on the CBCT image. The algorithm, which has been previously validated in a series of liver patients to achieve an accuracy of less than 2 mm in each direction, can therefore be used to map the tumor, defined on CT, onto the CBCT image.

To perform the deformable registrations, contoured livers were exported from the treatment planning system as binary masks that were converted into a tri-element surface mesh. A patient reference model was created from the CT planning image and then deformed into each successive representation of the patient. The deformation was performed using guided surface projection (HyperMesh; Altair Engineering, Troy, MI) of the surface of the reference mesh onto a surface generated from each CBCT liver. These displacements served as boundary conditions for the model. The displacement of the interior volume of the liver, including the motion of the tumor, was then solved using linear-elastic, small-deformation, finite element analysis (ABAQUS v6.8; D S Simulia, Providence, RI) (30). After the differences in patient position were resolved and a geometrically resolved view of the patient was created, a three-dimensional volumetric comparison of the liver and tumor representation on each image was performed (33).

Liver deformation

An evaluation of interfraction spatial differences of the liver surface was performed using MORFEUS to determine whether the liver shape was reproducible as a whole and whether there were trends in liver shape variability from day to day. The analysis included displacements taken over the population of nodes within the whole liver and each of eight geometric quadrants divided from the liver center of mass (COM), reported as standard deviation, maximum, and minimum for each patient. The quadrants were identified as superior–posterior right, superior–posterior left, superior–anterior–right, superior–anterior–left, inferior–posterior–right, inferior–posterior–left, inferior–anterior–right, inferior–posterior–right, and inferior–anterior–left.

GTV displacement

The GTV was delineated by an experienced radiation oncologist (L.A.D.) on contrast-enhanced planning CT scans. Using MORFEUS, a COM displacement of each GTV was determined for each available CBCT scan, based on the liver deformation after rigid liver-to-liver registration. A limitation of CBCT liver tumor position evaluation is the inability to visualize the tumor on CBCT. To overcome this, tumor motion was predicted by use of a COM displacement after deformable registration of the liver at each fraction (29).

RESULTS

We evaluated 83 CBCT scans from 16 patients with 30 GTVs (mean of 5 CBCT scans per patient; range, 1–6). The mean FB liver motion determined on fluoroscopy at treatment planning was 22 mm (range, 12–40 mm). On average, AC reduced SI motion by 11 mm (range, 4–28 mm), resulting in mean compressed liver motion due to respiration of 11 mm (range, 5–20 mm). Figure 1 shows interfraction liver changes for Patient 5, for three fractions, with the per-fraction CBCT liver contour (white) and planning CT liver contour (black).

Contour reproducibility

Three repeat liver contours were drawn on a single CBCT scan for each of three patients to determine the mean intraobserver contouring variability of 1.9 mm (SD, 0.7), 2.6 mm (SD, 0.6), 1.7 mm (SD, 0.3), and 3.4 mm (SD, 0.8) in the LR, AP, SI, and vector directions, respectively, for 95% of the liver surface.

Liver deformations

Residual liver deformations at treatment were determined after rigid alignment of the CBCT liver to the planning CT liver. Table 2 summarizes the residual CBCT liver deformations compared with the planning CT liver for all patients, in each of the left–right (LR), AP, and SI directions, as well as the percent liver volume deforming by greater than 5 mm. The mean, maximum, minimum, and median interfraction changes in liver shape after rigid liver-to-liver registrations are shown in Table 3. Table 3 also shows the interfraction GTV COM displacements predicted by the interfraction liver shape changes. For all patients, the absolute 95% liver maximum deformations in the LR, AP, and SI directions were 10.5 mm (SD, 2.2), 12.9 mm (SD, 3.6), and 5.6 mm (SD, 2.7), respectively. The maximum magnitude of change was seen in one outlier (Patient 4) who had consistently larger deformations than the others, with absolute 95% liver offsets of 10.5 mm (SD, 3.9), 12.9 mm (SD, 6.2), and 5.6 mm (SD, 2.0) in the LR, AP, and SI directions, respectively. The mean percent liver volume deforming by greater than 5 mm after rigid liver-to-liver registration in all patients was 8.7%, and it was 4.0% when the outlier was excluded (Table 2). Figure 2 is a deformation volume histogram generated by finding the maximum displacement over all patients and then setting the bin size to 0.25 mm. The deformation volume for each patient and each fraction was then determined, followed by the mean and standard deviation over all of those. Figure 2 is consistent with Table 2, which shows that the percent liver volume deformation (vector magnitude) greater than 3 mm is small in all patients.

When we evaluated liver deformations by quadrants (Fig. 3), over all patients and all fractions showed that the largest mean displacement occurred in the superior–anterior–right quadrant and the largest maximum displacement in the superior–anterior–left quadrant. However, the quadrant with the greatest frequency of per-patient, per-fraction largest mean displacements was the inferior–anterior–left quadrant (22 of 83 fractions). This portion of the liver is likely under the compression plate and/or adjacent to the stomach (Fig. 4). The quadrant with the next most frequent maximum variability was the superior–anterior–left quadrant (16 of 83 fractions), in the region of the liver sitting just above the stomach, suggesting that stomach filling reproducibility may affect the liver shape from day to day. Table 4 summarizes the population mean, maximum, and minimum per-quadrant residual liver deformations after rigid liver-to-liver registrations.

GTV displacement

The impact of liver deformation on GTV position after rigid liver-to-liver registration was predicted by use of the COM displacement of the GTV from the planning CT scan, based on liver deformations. The maximum changes in tumor COM were small (≤5 mm) in 15 of 16 patients, in all directions, with mean displacements of 1.4 mm (SD, 2.2), 2.1 mm (SD, 2.9), and 1.0 mm (SD, 1.1) in the LR, AP, and SI directions, respectively. In addition to consistently larger liver deformations, Patient 4 showed larger mean tumor COM displacements of 4.9 mm (SD, 3.4), 6.8 mm (SD, 4.8), and 1.7 mm (SD, 1.7) in the LR, AP, and SI directions, respectively. Table 3 shows the predicted tumor displacements after rigid liver-to-liver registrations for all patients. Figure 4 shows a single patient's deformable registration results and resultant GTV COM displacement for a single fraction. The color bars indicate the magnitude of displacement (in millimeters).

DISCUSSION

The benefits of AC in minimizing respiratory motion for SBRT have been described (18,22,34,35). The interfraction and intrafraction variability of respiratory liver motion in the SI direction is small (<2 mm) in most patients, as shown by Case (36), in 29 patients treated with ($n = 14$) and without ($n = 15$) AC, and Wunderink *et al.* (22) evaluated 12 subjects with varying levels of AC. These results are comparable to the reproducibility of exhale breath-held liver position (17,21,22,37). The current work shows that residual interfraction deformations in liver shape are also small, suggesting that there is little variability in liver shape under AC from day to day. However, the magnitude and frequency of residual deformations after liver-to-liver registration were difficult to predict, with the largest magnitude of deformation occurring in the superior–anterior quadrants and the greatest frequency of deformations occurring in the inferior–anterior– left quadrant. This is not unlike work by von Siebenthal *et al.* (23,24), who found the largest magnitude of respiratory liver motion of the right lobe of the liver in the superior region and the inferior– anterior portion of the liver showing the largest drift in the superior direction.

Online daily IGRT was performed for all patients correcting for rigid translations. Though not accounting for rotations and deformations, therapist-led image guidance may enhance accurate liver positioning. Despite the small deformations for most patients, for which rigid image guidance will suffice, larger deformations, like those for the outlier, cannot be compensated for.

The magnitude of residual changes in liver deformation and predicted liver tumor COM displacements after rigid liver-to-liver registrations under AC is similar to interfraction changes in patients with ABC breath hold. Hawkins *et al.* (28) reported a mean deformation magnitude of 1.8, 2.0, and 2.3 mm in 95% of the liver volume in the LR, AP, and SI directions, respectively, and a mean percent volume deformation greater than 5 mm of 2.9%, which are not significantly different from our findings (Tables 2 and 3). By use of a paired *t* test, liver deformations between the two populations resulted in *p* values of 0.1367, 0.1328, and 0.6248 in the LR, AP, and SI directions, respectively. Interestingly, this work showed the largest liver deformation and GTV displacement in the AP direction, whereas the work by Hawkins *et al.* showed the largest deformation for the patients in the SI direction. These results are consistent with work currently in press by this group evaluating liver tumor motion with and without AC by use of cine-MRI (38), which found that AP motion actually increased under AC in a minority of patients.

This is the first study using deformable registration to assess the change in liver shape and predicted GTV COM displacements over a course of treatment, comparing exhale respiratory sorted CBCT scans with exhale planning CT scans. A strength of the study is the number of patients ($n = 16$) evaluated at multiple fractions over the course of radiotherapy. In SBRT, where the dose delivered per fraction is high and the dose gradient steep, even small geometric errors in a single fraction can be dosimetrically relevant (26,39–41). The clinical consequence of such geometric offsets is the subject of ongoing research.

The method used to predict tumor motion using a COM displacement has been validated (30) and shown to have an accuracy of less than 2.0 mm (29,32), serving as a good predictor of tumor displacement in the absence of actual tumor visualization at the time of treatment delivery. *F* tests comparing the standard deviations for predicted tumor COM displacement in the exhale livers under AC from this cohort with the results of Brock *et al.* (29) in patients undergoing ABC breath-held radiotherapy showed no significant differences ($p = 0.404$ for LR, $p = 0.303$ for AP, and $p = 0.059$ for SI).

Using MRI, von Siebenthal *et al.* (42) reported that deformations of the liver due to respiratory motion, without AC, varied depending on the liver segment evaluated. Using "simple" geometric liver quadrants, our work indicated variability in liver quadrant deformations after rigid liver-to-liver registrations that may have been influenced by factors other than the compression plate (*e.g.*, stomach filling) based on the location of the most frequent deformations. We were unable to predict intrapatient and interpatient interfractional maximum displacements. Although factors such as stomach filling were not considered within the scope of this project, further investigations into the effects of stomach filling and its reproducibility are warranted. Work by Brock and colleagues (43–45) investigating accumulated dose to the target and surrounding normal tissues is currently ongoing.

Limitations of this work included the inability to clearly visualize or segment the tip of the left lobe and other organs at risk in some cases. As such, only liver contours were generated from the respiratory correlated CBCT scans. However, a strength of this work is that all registrations were biased to the region of the liver where the tumor(s) were located. This ensures that the reproducibility of liver positioning and shape in regions distal to the tumor has less consequence on the accuracy of treatment delivery and dosimetric impacts on treatment delivery. Using this strategy may account for local deformations that limit the use of whole-liver IGRT.

CONCLUSIONS

Liver deformations under AC were small in most patients. However, one patient had substantial deformation under AC, resulting in significant changes in GTV position, warranting efforts to ensure reproducibility and quality assurance of AC at the time of therapy. Offline deformable volumetric IGRT can be used to confirm the magnitude of deformation for patients undergoing liver SBRT. In the absence of real-time online deformable image registration tools, rigid translational registrations are adequate for treatment practice in most patients. Performing a rigid liver-to-liver alignment (by use of the contours generated from the planning scan overlaid onto the CBCT scan) can provide a quick and qualitative method of assessing residual deformation.

Acknowledgments

REFERENCES

1. Herfarth KK, Debus J, Lohr F, et al. Stereotactic single-dose radiation therapy of liver tumors: Results of a phase I/II trial. J Clin Oncol. 2001; 19:164–170. [PubMed: 11134209]

2. Herfarth KK, Debus J, Wannenmacher M. Stereotactic radiation therapy of liver metastases: Update of the initial phase-I/II trial. Front Radiat Ther Oncol. 2004; 38:100–105. [PubMed: 15458194]

3. Schefter TE, Kavanagh BD, Timmerman RD, Cardenes HR, Baron A, Gaspar LE. A phase I trial of stereotactic body radiation therapy (SBRT) for liver metastases. Int J Radiat Oncol Biol Phys. 2005; 62:1371–1378. [PubMed: 16029795]

4. Tse RV, Hawkins M, Lockwood G, et al. Phase I study of individualized stereotactic body radiotherapy for hepatocellular carcinoma and intrahepatic cholangiocarcinoma. J Clin Oncol. 2008; 26:657–664. [PubMed: 18172187]

5. Wulf J, Guckenberger M, Haedinger U, et al. Stereotactic radiotherapy of primary liver cancer and hepatic metastases. Acta Oncol. 2006; 45:838–847. [PubMed: 16982548]

6. Wulf J, Hadinger U, Oppitz U, Thiele W, Ness-Dourdoumas R, Flentje M. Stereotactic radiotherapy of targets in the lung and liver. Strahlenther Onkol. 2001; 177:645–655. [PubMed: 11789403]

7. Balter JM, Dawson LA, Kazanjian S, et al. Determination of ventilatory liver movement via radiographic evaluation of diaphragm position. Int J Radiat Oncol Biol Phys. 2001; 51:267–270. [PubMed: 11516877]

8. Davies SC, Hill AL, Holmes RB, Halliwell M, Jackson PC. Ultrasound quantitation of respiratory organ motion in the upper abdomen. Br J Radiol. 1994; 67:1096–1102. [PubMed: 7820402]

9. Balter JM, Lam KL, McGinn CJ, Lawrence TS, Ten Haken RK. Improvement of CT-based treatment-planning models of abdominal targets using static exhale imaging. Int J Radiat Oncol Biol Phys. 1998; 41:939–943. [PubMed: 9652861]

10. Aruga T, Itami J, Aruga M, et al. Target volume definition for upper abdominal irradiation using CT scans obtained during inhale and exhale phases. Int J Radiat Oncol Biol Phys. 2000; 48:465–469. [PubMed: 10974463]

11. Chen GT, Kung JH, Beaudette KP. Artifacts in computed tomography scanning of moving objects. Semin Radiat Oncol. 2004; 14:19–26. [PubMed: 14752730]

12. Rosu M, Dawson LA, Balter JM, McShan DL, Lawrence TS, Ten Haken RK. Alterations in normal liver doses due to organ motion. Int J Radiat Oncol Biol Phys. 2003; 57:1472–1479. [PubMed: 14630287]

13. Hara R, Itami J, Kondo T, et al. Stereotactic single high dose irradiation of lung tumors under respiratory gating. Radiother Oncol. 2002; 63:159–163. [PubMed: 12063005]

14. Lohr F, Debus J, Frank C, et al. Noninvasive patient fixation for extracranial stereotactic radiotherapy. Int J Radiat Oncol Biol Phys. 1999; 45:521–527. [PubMed: 10487580]

15. Negoro Y, Nagata Y, Aoki T, et al. The effectiveness of an immobilization device in conformal radiotherapy for lung tumor: Reduction of respiratory tumor movement and evaluation of the daily setup accuracy. Int J Radiat Oncol Biol Phys. 2001; 50:889–898. [PubMed: 11429216]

16. Wulf J, Hadinger U, Oppitz U, Olshausen B, Flentje M. Stereotactic radiotherapy of extracranial targets: CT-simulation and accuracy of treatment in the stereotactic body frame. Radiother Oncol. 2000; 57:225–236. [PubMed: 11054527]

17. Eccles C, Brock KK, Bissonnette JP, Hawkins M, Dawson LA. Reproducibility of liver position using active breathing coordinator for liver cancer radiotherapy. Int J Radiat Oncol Biol Phys. 2006; 64:751–759. [PubMed: 16458774]

18. Dawson LA, Balter JM. Interventions to reduce organ motion effects in radiation delivery. Semin Radiat Oncol. 2004; 14:76–80. [PubMed: 14752735]

19. Lax I, Blomgren H, Naslund I, Svanstrom R. Stereotactic radiotherapy of malignancies in the abdomen. Methodological aspects. Acta Oncol. 1994; 33:677–683. [PubMed: 7946448]

20. Blomgren H, Lax I, Naslund I, Svanstrom R. Stereotactic high dose fraction radiation therapy of extracranial tumors using an accelerator. Clinical experience of the first thirty-one patients. Acta Oncol. 1995; 34:861–870. [PubMed: 7576756]

21. Heinzerling JH, Anderson JF, Papiez L, et al. Four-dimensional computed tomography scan analysis of tumor and organ motion at varying levels of abdominal compression during stereotactic treatment of lung and liver. Int J Radiat Oncol Biol Phys. 2008; 70:1571–1578. [PubMed: 18374231]

22. Wunderink W, Mendez Romero A, de Kruijf W, de Boer H, Levendag P, Heijmen B. Reduction of respiratory liver tumor motion by abdominal compression in stereotactic body frame, analyzed by tracking fiducial markers implanted in liver. Int J Radiat Oncol Biol Phys. 2008; 71:907–915. [PubMed: 18514783]

23. von Siebenthal M, Szekely G, Lomax A, Cattin P. Inter-subject modelling of liver deformation during radiation therapy. Med Image Comput Comput Assist Interv. 2007; 10:659–666. [PubMed: 18051115]

24. von Siebenthal M, Szekely G, Lomax AJ, Cattin PC. Systematic errors in respiratory gating due to intrafraction deformations of the liver. Med Phys. 2007; 34:3620–3629. [PubMed: 17926966]

25. Dawson LA, Eccles C, Craig T. Individualized image guided iso-NTCP based liver cancer SBRT. Acta Oncol. 2006; 45:856–864. [PubMed: 16982550]

26. Dawson LA, Eccles C, Bissonnette JP, Brock KK. Accuracy of daily image guidance for hypofractionated liver radiotherapy with active breathing control. Int J Radiat Oncol Biol Phys. 2005; 62:1247–1252. [PubMed: 15990028]

27. Sonke JJ, Zijp L, Remeijer P, van Herk M. Respiratory correlated cone beam CT. Med Phys. 2005; 32:1176–1186. [PubMed: 15895601]

28. Hawkins MA, Brock KK, Eccles C, Moseley D, Jaffray D, Dawson LA. Assessment of residual error in liver position using kV cone-beam computed tomography for liver cancer high-precision radiation therapy. Int J Radiat Oncol Biol Phys. 2006; 66:610–619. [PubMed: 16966004]

29. Brock KK, Hawkins M, Eccles C, et al. Improving image-guided target localization through deformable registration. Acta Oncol. 2008; 47:1279–1285. [PubMed: 18766475]

30. Brock KK, Sharpe MB, Dawson LA, Kim SM, Jaffray DA. Accuracy of finite element model-based multi-organ deformable image registration. Med Phys. 2005; 32:1647–1659. [PubMed: 16013724]

31. Brock KK, Hollister SJ, Dawson LA, Balter JM. Technical note: Creating a four-dimensional model of the liver using finite element analysis. Med Phys. 2002; 29:1403–1405. [PubMed: 12148719]

32. Brock KK, Dawson LA, Sharpe MB, Moseley DJ, Jaffray DA. Feasibility of a novel deformable image registration technique to facilitate classification, targeting, and monitoring of tumor and normal tissue. Int J Radiat Oncol Biol Phys. 2006; 64:1245–1254. [PubMed: 16442239]

33. Brock KK, Nichol AM, Menard C, et al. Accuracy and sensitivity of finite element model-based deformable registration of the prostate. Med Phys. 2008; 35:4019–4025. [PubMed: 18841853]

34. Timmerman RD, Kavanagh BD, Cho LC, Papiez L, Xing L. Stereotactic body radiation therapy in multiple organ sites. J Clin Oncol. 2007; 25:947–952. [PubMed: 17350943]

35. Mendez Romero A, Zinkstok RT, Wunderink W, et al. Stereotactic body radiation therapy for liver tumors: Impact of daily setup corrections and day-to-day anatomic variations on dose in target and organs at risk. Int J Radiat Oncol Biol Phys. 2009; 75:1201–1208. [PubMed: 19386435]

36. Case R, Sonke J-J, Eccles CL, et al. Inter- and intra-fraction changes in amplitude of breathing motion in stereotactic liver radiotherapy. Int J Radiat Oncol Biol Phys. 2010; 77:918–925. [PubMed: 20207501]

37. Dawson LA, Brock KK, Kazanjian S, et al. The reproducibility of organ position using active breathing control (ABC) during liver radiotherapy. Int J Radiat Oncol Biol Phys. 2001; 51:1410–1421. [PubMed: 11728702]

38. Eccles CL, Patel R, Simeonov AK, Lockwood G, Haider M, Dawson LA. Comparison of liver tumor motion with and without abdominal compression using cine-MRI. Int J Radiat Oncol Biol Phys. 2010 In Press.

39. Dawson LA, Jaffray DA. Advances in image-guided radiation therapy. J Clin Oncol. 2007; 25:938–946. [PubMed: 17350942]

40. Song WY, Schaly B, Bauman G, Battista JJ, Van Dyk J. Evaluation of image-guided radiation therapy (IGRT) technologies and their impact on the outcomes of hypofractionated prostate cancer treatments: A radiobiologic analysis. Int J Radiat Oncol Biol Phys. 2006; 64:289–300. [PubMed: 16377417]

41. Song WY, Wong E, Bauman GS, Battista JJ, Van Dyk J. Dosimetric evaluation of daily rigid and nonrigid geometric correction strategies during on-line image-guided radiation therapy (IGRT) of prostate cancer. Med Phys. 2007; 34:352–365. [PubMed: 17278521]

42. von Siebenthal M, Szekely G, Gamper U, Boesiger P, Lomax A, Cattin P. 4D MR imaging of respiratory organ motion and its variability. Phys Med Biol. 2007; 52:1547–1564. [PubMed: 17327648]

43. Brock KK, Lee M, Eccles CL, Velec M, Moseley JL, Dawson LA. Deformable registration and dose accumulation to investigate marginal liver cancer recurrences [Abstract]. Int J Radiat Oncol Biol Phys. 2008; 72 Suppl.:S538.

44. Velec MJ, Moseley J, Dawson LA, Brock KK. Accumulated treatment dose for image guided liver radiotherapy using deformable image registration of 4D conebeam CT [Abstract]. Int J Radiat Oncol Biol Phys. 2008; 72 Suppl.:S149.

45. Velec MJ, Moseley J, Dawson LA, Brock KK. Importance of deformation including baseline shifts and breathing variation, on dose accumulation in liver SBRT [Abstract]. Int J Radiat Oncol Biol Phys. 2009; 75 Suppl.:S25–S26.
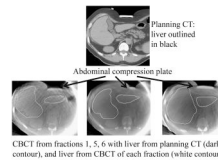
Fig. 1.
Example of changes in liver shape due to compression plate positioning and stomach filling in a single patient. Top, Planning computed tomography (CT) scan with liver contour (black). Bottom, Cone beam computed tomography (CBCT) scan from Fractions 1, 5, and 6, with liver contours from planning CT (black) and CBCT (white).
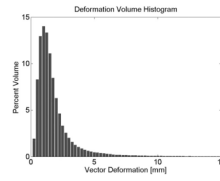
Fig. 2.
Deformation histogram showing magnitude of vector deformation vs. percent liver volume deformation.
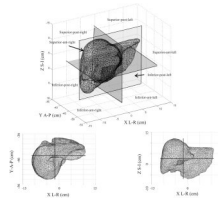
Fig. 3.
Geometric segments for evaluation of liver deformations under abdominal compression. post = posterior; ant = anterior; S-I = superior–inferior; A-P = anterior–posterior; L-R = left–right.

Fig. 4.
Results of deformable registration for a single patient fraction and resultant tumor center of mass displacement. Color bars indicate magnitude of displacement (in millimeters). SI = superior–inferior; AP = anterior–posterior; RL = right-left.

Table 1

Patient characteristics
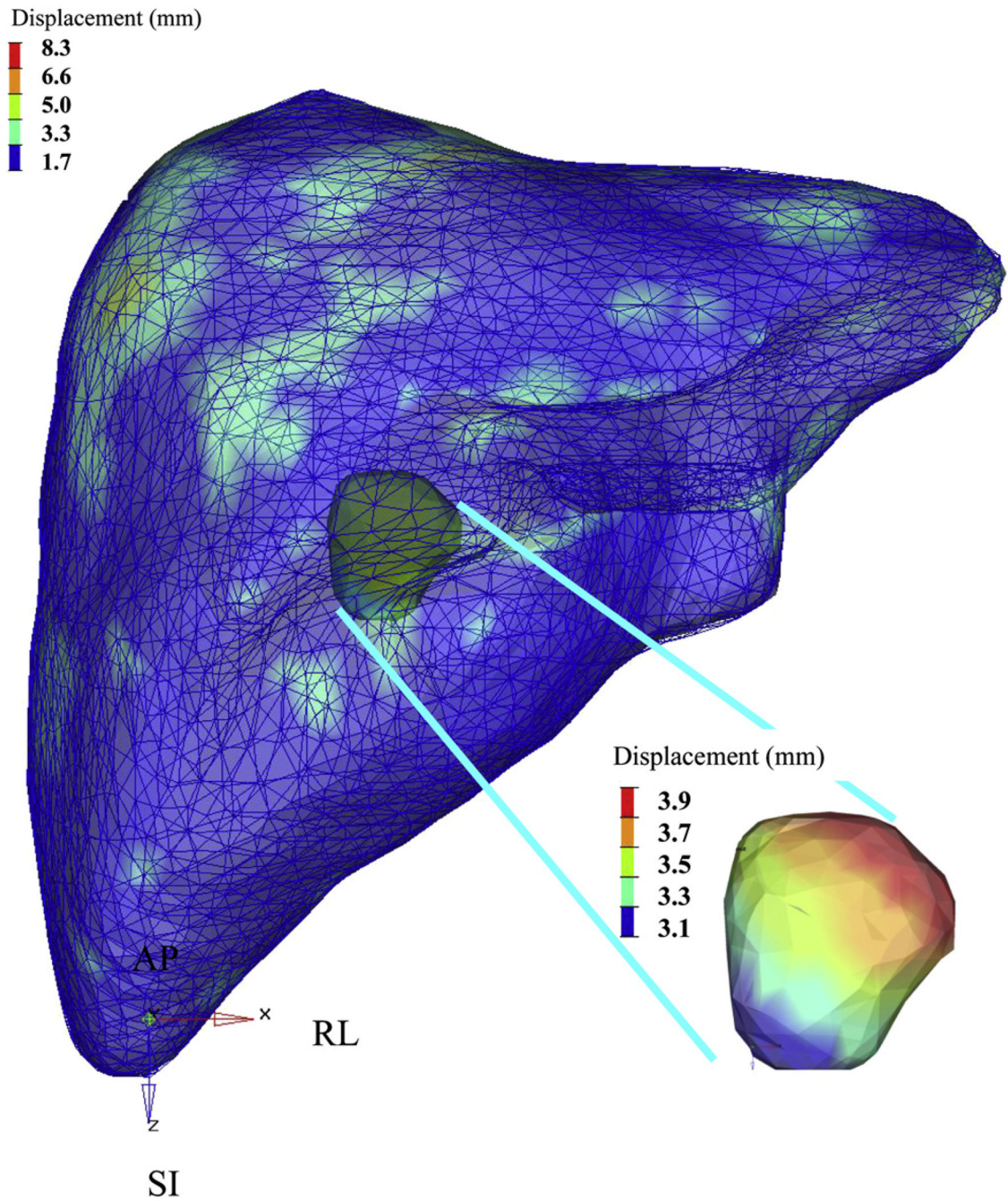
Patient No.	Sex	Diagnosis	Age (y)	No. of tumors	GTV (mL) (all GTVs)	Liver volume (mL)
1	M	HCC	58	1	242	2402
2	F	HCC	78	1	161	1933
3	F	Cholangio	79	1	147	1285
4*	F	Mets	51	7	6	1049
5	F	Mets	79	1	223	1574
6	F	Mets	67	1	426	1935
7	M	HCC	78	3	134	1935
8	F	Mets	82	1	11	1495
9	M	Mets	75	5	45	1240
10	F	Mets	68	1	11	1300
11	F	HCC	78	4	346	1856
12	M	HCC	75	4	137	1583
13	M	Mets	74	1	12	1951
14	F	Mets	76	1	4	1660
15	M	HCC	82	1	170	1158
16	F	Mets	75	1	26	1194
All patients						
Mean			73.4	2.1	131.3	1596.9
Maximum			82.0	7.0	426.0	2402.0
Minimum			51.0	1.0	4.2	1049.0
SD			8.6	1.9	129.1	379.9

Abbreviations: GTV = gross tumor volume; HCC = hepatobiliary carcinoma; Cholangio = cholangiocarcinoma; Mets = metastatic liver disease.

*
Outlier.

Table 2

Population mean and maximum deformations of 95th percentile of CBCT liver when compared to planning CT represented as percent liver volume deforming more than 3, 5 or 10 mm

	Deformation of 95% liver volume			% Liver deformation >5 mm
	LR (mm)	AP (mm)	SI (mm)	
Patient No.				
1	3.3	5.1	2.4	6.6
2	2.3	3.1	3.7	5.4
3	2.4	2.9	2.9	0.3
4	10.5	12.9	5.6	82.4
5	3.0	3.0	3.5	2.5
6	1.5	2.1	2.1	1.2
7	2.8	4.2	2.3	8.3
8	2.0	3.2	3.4	3.4
9	2.5	4.3	2.4	8.5
10	1.5	2.4	2.1	2.8
11	1.7	2.6	2.6	2.4
12	1.2	2.1	1.6	0.5
13	1.6	2.1	1.5	0.4
14	2.6	2.7	3.1	5.6
15	1.7	2.1	2.0	1.2
16	3.5	3.5	2.7	10.8
Population mean[*]	2.8	3.7	2.7	8.7
Population maximum[*]	10.5	12.9	5.6	15.9

Per-patient mean deformation of 95% liver CBCT liver volume was determined by use of all available CBCT scans (1–6 per patient).

Abbreviations: CBCT = cone beam computed tomography; CT, computed tomography; LR = left–right; AP = anterior–posterior; SI = superior–inferior.

[*] Including outlier.

Table 3

Magnitude and direction of interfraction liver shape (95th percentile) changes for all patients and resultant GTV COM displacements after rigid liver-to-liver registration described as absolute and non-absolute minimum, maximum, median, mean, and standard deviation of means in left–right (LR), anterior–posterior (AP), superior–inferior (SI), and vector directions

	LR (mm)	AP (mm)	SI (mm)	Vector (mm)	Absolute LR (mm)	Absolute AP (mm)	Absolute SI (mm)
Liver							
Mean	1.9	2.2	1.5	4.6	2.8	3.6	2.7
SD	1.9	1.5	1.1	3.1	2.2	3.6	2.7
Maximum	8.6	5.0	4.8	15.6	10.5	12.9	5.6
Minimum	0.5	−1.6	0.5	1.7	1.2	2.1	1.0
Median	1.4	2.2	1.1	4.1	2.5	2.9	2.5
Tumor							
Mean	−0.3	−0.4	−0.5	0.00	0.9	1.3	0.8
SD	0.6	2.1	0.8	0.00	1.3	1.8	0.7
Maximum	8.6	5.4	6.7	0.5	14.6	16.9	6.7
Minimum	−14.6	−16.9	−3.5	0.00	0.00	0.1	0.00
Median	−0.3	0.5	−0.6	0.00	0.6	1.0	0.8

Abbreviations: GTV = gross tumor volume; COM = center of mass; LR = left–right; AP = anterior–posterior; SI = superior–inferior.

Table 4

Population per-quadrant liver absolute mean, minimum, maximum, and SD of vector displacements

Quadrant	Mean (mm)	SD (mm)	Maximum (mm)	Minimum (mm)
Superior–posterior–right	2.6	1.1	5.9	0.7
Superior–posterior–left	2.3	1.0	5.2	0.5
Superior–anterior–right	2.7	1.3	7.0	0.5
Superior–anterior–left	2.2	1.4	7.9	0.2
Inferior–posterior–right	1.9	0.9	4.3	0.2
Inferior–posterior–left	2.2	0.9	4.5	0.4
Inferior–anterior–right	2.2	1.4	9.9	0.3
Inferior–anterior–left	1.5	0.8	3.7	0.2